Journal Pre-proofs

High temperature flow synthesis of iron oxide Nanoparticles: Size tuning via reactor engineering

Maximilian O. Besenhard, Liudmyla Storozhuk, Alec. P. LaGrow, Luca Panariello, Adam Maney, Sayan Pal, Céline Kiefer, Damien Mertz, Le Duc Tung, Martin R. Lees, Nguyen Thi Kim Thanh, Asterios Gavriilidis

Please cite this article as: M.O. Besenhard, L. Storozhuk, c.P. LaGrow, L. Panariello, A. Maney, S. Pal, C. Kiefer, D. Mertz, L.D. Tung, M.R. Lees, N.T.K. Thanh, A. Gavriilidis, High temperature flow synthesis of iron oxide Nanoparticles: Size tuning via reactor engineering, *Chemical Engineering Journal* (2023), doi: https://doi.org/10.1016/j.cej.2023.144542

High Temperature Flow Synthesis of Iron Oxide Nanoparticles: Size Tuning via Reactor Engineering

Maximilian O. Besenhard,[a],* Liudmyla Storozhuk,[d,e] Alec. P. LaGrow,[c] Luca Panariello,[a] Adam Maney,[a] Sayan Pal,[a] Céline Kiefer,[b] Damien Mertz,[b] Le Duc Tung,[d,e] Martin R. Lees,[f] Nguyen Thi Kim Thanh,[d,e] Asterios Gavriilidis[a],*

[a] *Department of Chemical Engineering, University College London, London, WC1E 7JE, U.K.*

[b] *Institut de Physique et Chimie des Matériaux de Strasbourg, BP 43, 67034, Strasbourg, France*

[c] *Institute for Science and Technology Graduate University, Okinawa 904-0412, Japan*

[d] *Biophysics group, Department of Physics and Astronomy, University College London, London, WC1E 6BT, U.K.*

[e] *UCL Healthcare Biomagnetics and Nanomaterials Laboratories, 21 Albemarle Street, London, W1S 4BS, U.K.*

[f] *Superconductivity and Magnetism Group, Physics Department, University of Warwick, Coventry CV4 7AL, U.K.*

* Corresponding authors: m.besenhard@ucl.ac.uk, a.gavriilidis@ucl.ac.uk

KEYWORDS: Continuous synthesis, flow chemistry, thermal decomposition, iron oxide nanoparticles, high temperature reactor

Abstract:

Batch thermal decomposition syntheses of iron oxide nanoparticles (IONPs) provide precise control of particle properties, but their scalability and reproducibility is challenging. This is addressed in this work via a versatile gram-per-day scale high temperature flow reactor with adjustable temperature profiles through three individual stages operated between 180 °C and 280 °C. The tuneable temperature profiles in combination with self-seeded growth methods made it possible to synthesise IONPs between 2 and 17 nm (a size increase that corresponds to a > 600 fold particle volume increase) at production rates of several g_{IONP} per day. The precursor solutions contained only iron(III) acetylacetonate in a polyol solvent and no nucleation or growth inhibitors, oxidation or reducing agents, ligands or others were added. This broad size range covers most biomedical applications and is of special interest for T_1 MRI contrast agents (2-5 nm), as well as for magnetic hyperthermia cancer therapy (>10 nm). The potential of the IONPs produced in such applications was demonstrated by the small IONPs' longitudinal relaxivity > 16 mM^{-1} s^{-1} at a transversal/longitudinal relaxivity ratio < 2.5 and the large IONPs' increase in the specific absorption rate to 180 W/g_{Fe}. In addition, the polyol method employed allowed for simple ligand exchange with biocompatible sodium tripolyphosphate to make the IONPs stable in water, thus rendering them suitable for biomedical applications. The continuous high temperature process presented shows how to control the particle size not via the chemistry (e.g., chemical additives affecting the particle size through the surface chemistry), but engineering parameters, i.e., reactor temperature profiles, reagent addition sequences and seeded growth strategies.

Introduction

Magnetic nanomaterials are well established for many applications including waste water treatment,[1] mechatronics,[2,3] and catalysis,[4] but are of special interest for biomedicine. Biomedical applications such as contrast agents for magnetic resonance imaging (MRI),[5–7] or the exploitation of magnetic nanoparticle heating in alternating magnetic fields for hyperthermia cancer treatment,[8–10] antimicrobial materials,[11,12] and drug delivery[13,14] use superparamagnetic iron oxide nanoparticles (IONPs) of the bio-compatible maghemite (γ-Fe_2O_3) and/or magnetite (Fe_3O_4) phases.

For all applications, the particle size is crucial, making it the focus of most reports on magnetic nanomaterial synthesis. IONPs ≤ 5 nm have recently attracted attention as T_1 contrast agents for MRI,[7,15] whereas larger particles (or clusters) are favoured for T_2 contrast enhancement.[16,17] Magnetically induced hyperthermia requires particles > 10 nm, as they favour heat generation in alternating fields.[18–20] For all biomedical applications, the colloidal stability is essential. Hence, IONP sizes must not exceed the superparamagnetic limit (the particle's magnetisation direction flips randomly avoiding agglomeration due to magnetic attraction), which is ~30/25 nm for maghemite/magnetite.[21] Catalytic applications benefit from the high surface to volume ratio of small IONPs too (if the iron oxide phase is active),[22] but larger particles ease magnetic recovery[23–25] for IONP supported nano-catalysts.[26,27]

As the range of applications is broad and not only size matters (e.g., purity, shape, crystallinity, surface chemistry), the variety of synthetic procedures is vast. Aqueous precipitation methods are the most common syntheses due to cheap and environmentally friendly precursors, simple experimental procedures, as well as advantages from a regulatory perspective for biomedical applications.[28,29] Their control of IONP size, however, is limited (with exceptions[30,31]).

Thermal decomposition syntheses, on the other side, are well established for accurate nanoparticle size (and shape) control for IONP synthesis.[32–38] These high temperature syntheses typically use metalorganic precursors such as iron carboxylate which decomposes at temperatures >200 °C in high boiling point organic solvents. In the past, non-polar solvents were typically used, but polyol methods (i.e., where a polar polyol is the high boiling point solvent and acts as reducing agent and stabiliser)[39–42] gained more interest over the years as their simpler ligand exchange procedures and better biocompatibility compared to other solvents make them highly relevance especially for biomedical applications.[6,41,43,44] For all high boiling point solvents, particle size control is achieved through additives (i.e., chemicals promoting or inhibiting nucleation or growth), changes in the precursor concentration or solvent composition, seeded growth strategies, reaction temperature and time, as well as temperature profile and especially heating rate.[34,45–47] The sensitivity of IONP properties to these parameters makes thermal decomposition syntheses well-suited for particle engineering, but imposes severe challenges regarding reproducibility and scalability. Furthermore, particle size control for polyol methods remains challenging with most protocols yielding (rather polydisperse, for high temperature methods) IONPs of 6-9 nm. Synthesis of > 9 nm IONPs in polyols is achieved by additives, alterations of the solvent composition and/or via lengthy (hours-days) protocols commonly followed by post-processing in autoclaves.[6,44,48,49]

As discussed previously,[50] flow reactors can overcome the scalability limitations of high temperature syntheses due to their inherent continuous operation and larger surface-area-to-volume ratios (compared to batch reactors) accelerating heat transfer. In addition, flow reactors facilitate reproducible production via accurate control of synthetic conditions (especially the temperature profile) and by minimising the operator influence. The temperatures required for high temperature IONP syntheses, however, impose challenges for flow reactors regarding the reactor materials, operation and sample collection, and fouling. Hence, studies demonstrating the potential of continuous IONP production via thermal decomposition emerged only recently using flow reactors comprising metallic, heat resistant plastic, or glass tubing heated via oil baths or electric heaters or metallic chip reactors.[50–57] Although the designs differ, these reactors share the same concept. One precursor solution is pumped through tubing/channels heated at a single (or two)[52] temperature above the precursor decomposition temperature. Most commonly used were polyol methods, which confirms their

importance in high temperature IONP synthesis, but also suggests a better translatability to flow (either from a chemistry or reactor engineering perspective). What all studies demonstrated is that i) synthesis times can be reduced significantly in flow, and that ii) the particle sizes are smaller compared to their batch equivalent. Both are expected as the reaction conditions differ drastically. Most importantly, the heating rate (i.e., the temporal temperature increase to and above the precursor decomposition temperature)is distinctly higher in flow, which is expected to enhance nucleation and yield more but smaller IONPs.[58,59] This explains the restricted control of particle size and distribution (posing challenges especially for the synthesis of > 10 nm particles), achieved via high temperature flow reactors.

To sum up, high temperature batch procedures cannot be translated directly into flow, but flow reactors facilitate novel synthetic procedures. This translatability problem is not only inherent in the showcased high temperature IONP polyol synthesis, but for many other important high temperature nanomaterial syntheses such as quantum and carbon dots,[60,61] metallic nanoparticles,[62,63] silica nanoparticles,[64] or other metal oxides.[65]

Thus, particle size control in flow remains challenging and needs new synthetic procedures which require versatile high temperature flow reactors.

To overcome this limitation, we present a modular gram-per-day scale high temperature flow reactor for the continuous and reproducible production of IONPs using a polyol method. The flexible temperature profiles set by three individual heating stages (operated between 180 °C and 280 °C) in combination with self-seeded growth methods made it possible to synthesize IONPs in the range of 2-17 nm. The precursor solution used was nothing more than the iron(III) acetylacetonate precursor in the polyol solvent without any nucleation and/or growth inhibitors.

In the following, we first describe the reactor design and then showcase continuous IONP syntheses at single and two heating stages (and their potential for T_1 MRI contrast agents), as well as three stages with seeded growth (with potential for magnetically induced hyperthermia).

Materials and methods

Chemicals and solution preparation

The iron(III) acetylacetonate (Fe(acac)$_3$, 99.9%; Merck Millipore) and triethylene glycol (TREG, 99%; Sigma-Aldrich) used for the precursor solution, as well as ethyl acetate (EtAc, 99.8%; Sigma-Aldrich), sodium tripolyphosphate (STTP, Alfa Aesar), and polyacrylic acid (PAA with Mw = 1,800 Da; Sigma-Aldrich), nitric acid (70% HNO$_3$ for ICP, 99.999% trace metal basis; Sigma-Aldrich), and the Fe standard for ICP (TraceCERT®, Sigma-Aldrich), used for IONP synthesis, purification and analysis were used as received. Details of all chemicals used, including product numbers are listed in **Table S1** in the supplementary information (SI).

The 0.033 M Fe standard (if not specified otherwise) precursor solution was prepared by dispersing 1.18 g Fe(acac)$_3$ in 100 ml of TREG, which became a homogenous (dark red) solution after heating above 80 °C. The precursor solution was nitrogen purged at 120 °C for > 40 min to remove water, dissolved oxygen, and assure the complete dissolution of Fe(acac)$_3$. Subsequently, the precursor solution was cooled to 100 °C and kept at this temperature throughout the reactor operation to maintain a homogenous solution (i.e., to keep the precursor dissolved and maintain a uniform concentration).

High temperature flow reactor design and operation

A schematic of the high temperature flow reactor is shown in **Figure 1**. As described previously,[50] a pressure pump (OB1, Elveflow), operated with nitrogen, guaranteed an inert atmosphere and conveyed the precursor solution through the reactor. To feed two precursor solution streams, a dual-channel system was used feedback-controlling the pressure channels separately using two flow meters (2 x Elveflow MFS4). Both

flowmeters were heated to 40 °C to reduce the risk of deposit formation in their measurement capillaries. For gas-liquid segmentation, nitrogen was fed via a mass flow controller (0.1-5 ml$_s$/min EL-FLOW Prestige, Bronkhorst).

The high temperature reactor comprised of three individual temperature stages (Stage 1-3), each with a cylindrical alumina block at its core being heated via a central cartridge heater. The tubing used to withstand the high temperatures was 1/8" stainless steel (SS) tubing with a 2 mm inner diameter (ID). This tubing was internally coated with Dursan® (SilcoTek), a corrosion and fouling resistant functionalised amorphous silica coating which increased the oleo and hydrophobicity, as used previously.[50] Likewise, all the SS elements connecting SS tubing were coated internally (Swagelok fittings coated with Dursan® or SilkoNert® by SilcoTek). To test the fouling resistance of Dursan® coated SS, coated metal coupons were immersed in the reaction media during two syntheses, i.e., one synthesis using a polyol solvent and one using a benzaldehyde/1-octadecene solvent (see SI section 1.2). This batch study proved the fouling resistance of the coating selected, and demonstrated the advantage of polyol methods (**Figure S1**) showing low fouling likelihood on metal/glass and indicating that polyol methods are easier to translate to flow.

For optimum heat transfer, the tubing was hosted in matching semi-spherical groves carved into the alumina blocks. The tube was jacketed with aluminium clamps with the counterpart semi-spherical grooves to perfectly embed the tubing (see **Figure S2a**). The clamps had cavities to place custom-made thermocouples in close proximity to the tubing. Each heating stage was fixed to a SS stand via thin SS bolts to minimise heat transfer to the stand and insulated with several layers of silicate wool (Superwool fibre, RS-PRO; ENV 1094-3 standard) for safe and energy efficient operation at high temperatures.

The tube length on each heating stage varied (Stage 1: 1 m, Stage 2: 4 m, Stage 3: 10 m; 15 m in total) to flexibly set the temperature profile. For example, a short nucleation step followed by longer growth and annealing steps. For connections between the precursor solution containing flasks, flow meters, collection vessels, etc. 1/16" (= 1.58 mm) or 1/8" PTFE tubing (1 mm or 2 mm ID) was used with standard plastic connectors (Upchurch Scientific) made of ETFE or PEEK.

The SI provides details of all components and materials used (see **Table S2**), pictures of the high temperature reactor (tubing and groves, the multistage reactor **Figure S2d**, the complete set-up in operation **Figure S3**), infrared camera images of the heated reactor stages (see **Figure S4**), as well as details on the reactor manufacturing (see SI section 2.2).

Characterisation

The IONP diameter D_{TEM} was determined from transmission electron microscope (TEM) images captured with a JEM 1200 EX (JEOL) with a tungsten filament and operated at 120 kV. D_{TEM} refers to the diameter of a circle with the same area as a polygon fitted manually around the particle edges. The diameters and errors reported are average values (for >100 particles) with the corresponding standard deviations. Aberration corrected high resolution TEM (HRTEM) and high angle annular dark field scanning transmission electron microscopy (HAADF-STEM) was performed using a Titan Themis 60-300 (FEI, Hillsborough) equipped with an image and probe corrector, and operated at 200 kV.
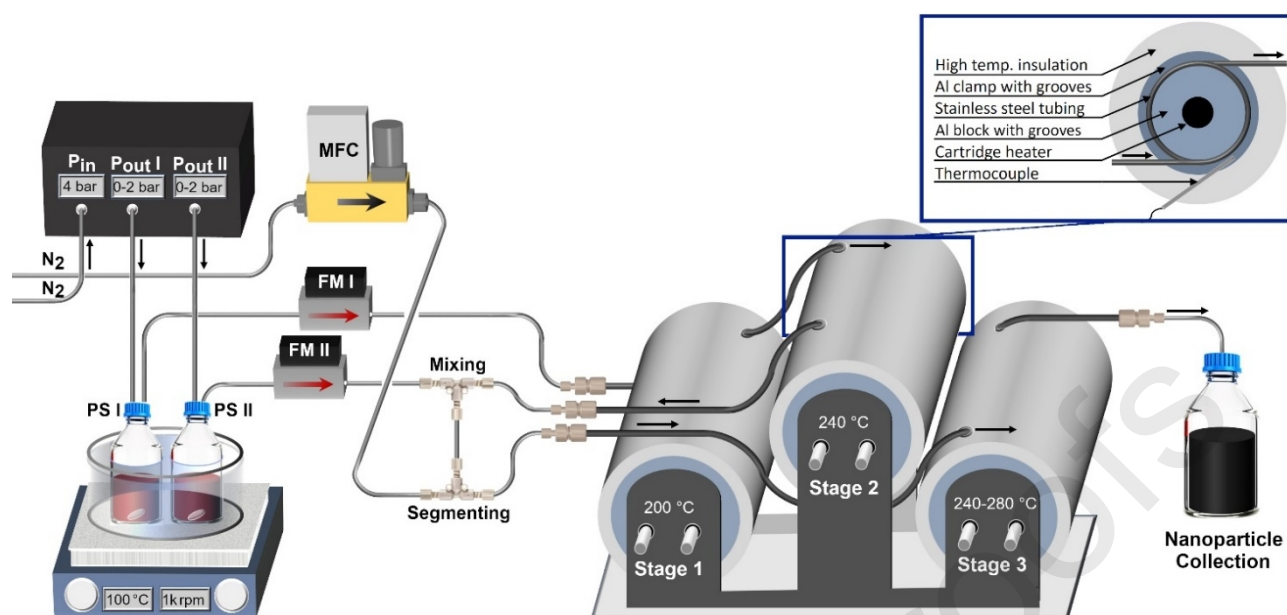
Figure 1: Schematic of the continuous thermal decomposition synthesis set-up. MFC: mass flow controller, FM: flowmeter, PS: precursor solution.

The hydrodynamic diameter D_h was obtained by dynamic light scattering (ZEN 3600, Malvern Instruments) at 22 °C after sufficient dilution with the samples' solvent, i.e., either TREG or deionised water. The X-ray diffraction (XRD) patterns of washed and dried samples were recorded using a $Co_{K\alpha}$ radiation source operated at 40 mA and 40 kV (Malvern Instruments, PANalytical X'Pert3). Magnetisation hysteresis curves were obtained via a superconducting quantum interference device (SQUID) magnetometer (MPMS, Quantum Design). To obtain the IONP weight and normalise SQUID measurements, thermogravimetric analysis (TGA) was performed for dried samples from 25 °C to 600 °C at 5 °C/min (SDT 600, TA instruments).

The precursor conversion X was determined via UV-Vis spectroscopy (USB 2000+, Ocean Optics) by diluting IONP solution in isopropyl alcohol to measure absorption in the linear Beer-Lambert regime as described previously,[50] using the precursor and sample solution absorbance at 273 nm; $X \, [\%] = (1 - A_{sample}/A_{prec.}) \times 100$. It should be noted that the conversion might be underestimated for high conversions, as the particles formed do also contribute to the absorption at 273 nm. The concentration of Fe in the form of particles ($mg_{Fe\text{-}IONP}$/ml) in IONP solutions was measured *via* microwave plasma atomic emission spectroscopy (MP-AES 4210, Agilent), with samples prepared as described previously.[30]

The longitudinal ($r_1 \, [mM^{-1} \, s^{-1}]$) and transversal ($r_2 \, [mM^{-1} \, s^{-1}]$) relaxivities were obtained from magnetic relaxation rates measurements at different Fe concentrations ($C_{Fe} \, [mM]$, quantified also by relaxometry) via time-domain nuclear magnetic resonance (Minispec 60 contrast agent analyser, Bruker) at a field frequency and strength of 60 MHz and 1.41 T. The particles' heating abilities in an alternating magnetic field were measured calorimetrically (G2 driver D5 series, nB nanoScale Biomagnetics) and quantified by the specific absorption rate (SAR) and the field and frequency normalised intrinsic loss parameter (ILP).[66] Details of the relaxivity and heating performance measurements were described previously.[30,43]

Results and discussion

Single-stage thermal decomposition synthesis

To study the particle formation onset, the high temperature flow reactor (HTFR) was operated using Stage 1 only, which was heated at and above the precursor decomposition temperature of 180 °C.[67] The precursor solution fed at 0.5 ml/min was segmented with N_2 at 0.6 ml_s/min for plug flow like behaviour (see **Figure 2a**). The pressure pump recordings revealed no fluctuations throughout the operation, confirming a stable flow process (see **Figure S15**).

Due to the rapid heating and cooling in the HTFR, the precursor solution was kept at the set temperature for only ~2 min (at 0.5 ml/min precursor solution feed and segmented flow, accounting for the gas expansion). Such short temperature intervals are intrinsic to flow reactors and can be achieved in batch only via hot injection followed by rapid coolant addition. TEM analysis could not reveal particles at 180 °C, but showed particle formation at 200 °C, i.e., the next higher temperature used (see **Figure 2b**). The particles formed at 200 °C and 220 °C were extremely small (D_{TEM} < 3 nm) and therefore hard to size via TEM. Increasing the temperature to 240 °C and 260 °C increased the IONP size to D_{TEM} = 3.4 nm and 4.6 nm respectively.

The HRTEM image of the IONPs synthesised at 200 °C showed a single crystalline particle of ~2.5 nm in diameter. The atomic spacing matched the inverse spinel structure of magnetite/maghemite viewed down the [310] zone axis (see **Figure 2c** and insert). Additional HRTEM images of the 200 °C and 220 °C syntheses are shown in **Figure S6**&**7**. XRD of the < 3 nm IONP synthesised at 220 °C confirmed that particles were magnetite/maghemite (see **Figure 2d**). The smaller (and less concentrated, see below) particles synthesised at 200 °C could not be separated from solution for XRD. UV-Vis spectroscopy for conversion analysis (see **Figure 2e**) showed a decreasing absorbance from 180 °C to 260 °C corresponding to a 29% (i.e., conversion was observed, despite TEM showing no particles), 53%, 76%, 93% and 96% conversion. For the 0.5 ml/min precursor solution fed, this equates to hourly and daily IONP production rates of 0.04-0.07 g_{IONP}/h and 1-1.8 g_{IONP}/d of magnetite. Although higher conversions at higher temperatures were in line with the IONP size increase, classic additive growth only (i.e., surface growth via monomer addition), which was suggested previously for polyol methods,[6,48] is unlikely. For example, the ~6 fold volume increase from 2.6 nm at 220 °C to 4.6 nm particles at 260 °C can't be explained solely by higher conversions (from 76% to 96%). Hence, particle growth (> 3 nm) seems likely via coalescence, which is in line with previous studies on IONP and other nanoparticle systems.[50,68–71]

The IONPs synthesised using a single stage set-up are significantly smaller compared to batch polyol methods yielding 7-9 nm.[39,41] This size reduction was assigned to the rapid heating and agrees with other flow studies.[52,55,72] The synthesis of IONPs ≤ 3 nm without any growth inhibiting additives, however, is unique.
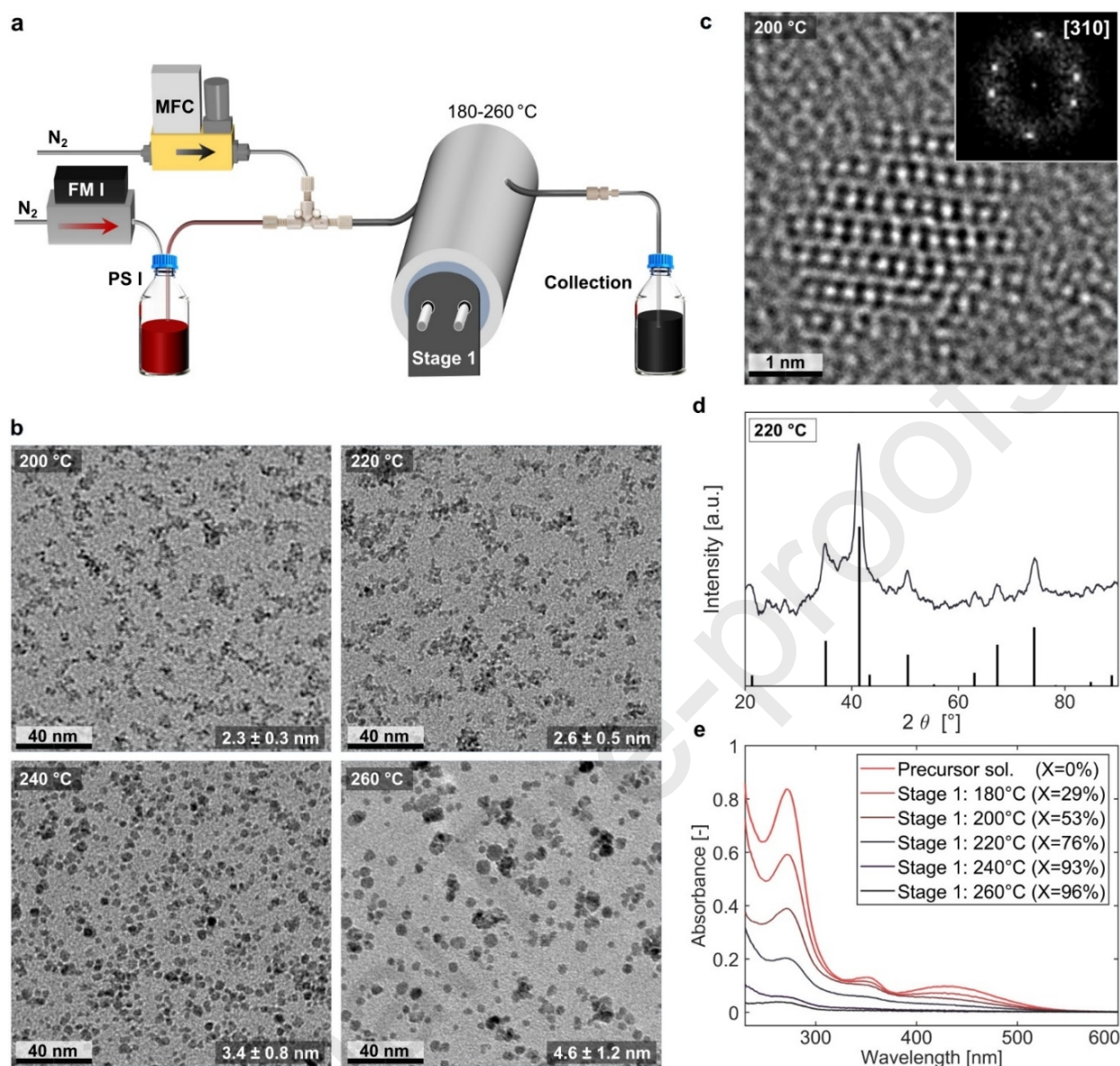
Figure 2:(a) Schematic of single-stage reactor set-up. (**b**) TEM images of IONPs synthesised via single stage (Stage 1) process, set between 200 °C and 260 °C. (**c**) HRTEM image of the ultra-small (≤ 3 nm) IONPs synthesised at Stage 1 at 200 °C. The inset shows the fast Fourier transformation (FFT) indexed to a magnetite/maghemite [310] zone axis, taken from the particle. (**c**) XRD pattern of IONPs synthesised with Stage 1 at 220 °C. The bars at the bottom refer to the inverse spinel structure (magnetite: PDF ref. 03-065-3107). (**e**) UV-Vis spectra of precursor and IONP solutions diluted in IPA.

Two-stage thermal decomposition synthesis

To better separate nucleation and growth, as well as to increase the reaction time, a two-stage HTFR set-up was used (see **Figure 3a**). Stage 1 (~2 min residence time for the 0.5 ml/min precursor solution feed and segmented flow used, accounting for the gas expansion) was operated at 200 °C to initiate nucleation and was followed by Stage 3, which had the longest tube length, to increase the residence time (~20 min) at 200 °C or 240 °C. The pressure pump recordings confirmed a stable flow process (see **Figure S16**). The increased residence time in Stage 3 did not yield a further increase in conversion at higher temperatures (93% at 240 °C, same as using Stage 1 only) but at lower temperatures (88% at 200 °C, compared to 53% using Stage 1 only, see **Figure S12**). This equates to respective IONP production rates of 1.7 and 1 g$_{IONP}$/d.

7

XRD confirmed that also using the two-stage HTFR the IONPs synthesised were magnetite/maghemite (see **Figure S13**). TEM analysis (see **Figure 3b**) showed that the IONP size increased to D_{TEM}= 3.2 ± 0.7 nm, 3.4 ± 0.7 nm and 6.2 ± 1.0 nm compared to the 200 °C, 220 °C and 240 °C single stage synthesis. At 240 °C the polydispersity (here quantified via the relative standard deviation, RSD = std./mean) decreased significantly, i.e., from RSD = 23% (single stage) to RSD = 15% for the two-stage process. This lower RSD (compare 240 °C IONPs in **Figure 2b** and **3b)** indicates a better separation between nucleation and growth. The different particle sizes obtained at 240 °C using the two-stage HTFR, despite a comparable conversion in the single-stage HTFR, indicate growth via coalescence too. In line with growth via coalescence, the larger particle size obtained in the two-stage HTFR can be assigned to the longer residence time allowing for more collisions, hence further growth.
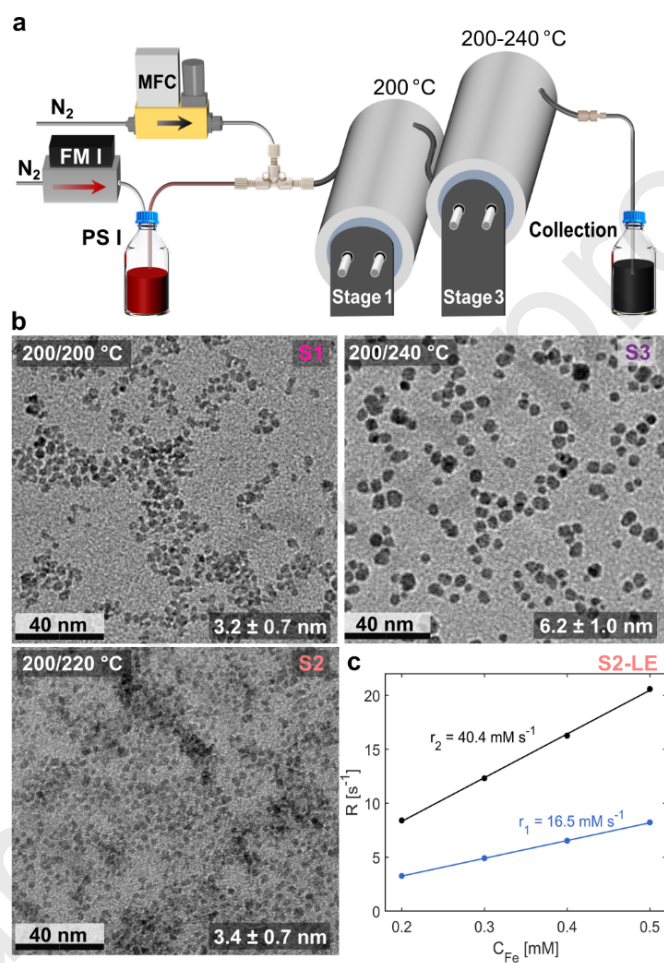

Figure 3: (**a**) Schematic of two-stage reactor set-up. (**b**) TEM images of IONPs synthesised via two-stage process with Stage 1 at 200 °C and Stage 3 at 200 °C (S1), 220 °C (S2) and 240 °C (S3). (**c**) The transversal (black line) and longitudinal (blue line) magnetic relaxation rates (R) vs. consecutively diluted iron concentrations (C_{Fe}) of ligand exchanged (LE) and dialysed aqueous IONP solution (S2) are used to determine the relaxivities r_2 and r_1 (i.e., the slope).

The two-stage HFTR operated at lower temperatures (≤ 220 °C) made it possible to synthesise ~3 nm magnetite/maghemite IONPs at a considerable conversion (≥ 88%). Although slightly bigger than the IONPs synthesised via the single-stage HTFR (2.3-2.6 nm), these IONPs still have an extremely high surface-to-volume ratio and the final IONP concentration was higher, which simplified separation and purification for further testing. This makes these ~3 nm IONPs a promising candidate for catalytic applications as well as T_1 (= longitudinal) MRI contrast agents. Before testing their potential as contrast agent using sample S2 (**see Figure 3**), however, the ~3 nm IONPs had to be rendered stable in water. Since a polyol method was used,

8

this was possible via a simple one-pot ligand exchange protocol using sodium tripolyphosphate.[43] Details of the ligand exchange and dialysis protocol used, as well as DLS and TEM studies confirming a successful exchange, are provided in the SI (section 4). The ligand exchanged and dialysed aqueous IONP solution S2-LE (synthesised with Stage 3 at 220 °C) was tested for its relaxation rate at different concentrations to determine the relaxivities (see **Figure 3c**). This evidenced the ~3 nm IONPs' potential as T_1 contrast agents, with S2-LE showing a longitudinal relaxivity of $r_1 > 16$ mM^{-1} s^{-1} and a transversal/longitudinal ratio of $r_2/r_1 < 2.5$. These values are already amongst the best values reported,[7,73] without any optimisation of the ligand exchange protocol or the synthesis itself. This, plus the advantageous production in flow showcased the potential of the HTFR for IONP contrast agent synthesis.

To increase the particle size further, the two-stage synthesis was repeated adding PAA to the precursor solution, as this yielded well-defined 20-30 nm multicore nanoflowers (~10 nm core size) in previous batch studies.[43] Both PAA concentrations tested, 33 and 0.33 mM (i.e., the same Fe(acac)$_3$/PAA ratio as used in batch), however, resulted in severe reactor fouling as indicated by the pressure and flow rate fluctuation of the pump system (see **Figure S17**). Hence, the PAA process could not be considered as robust. Although PAA addition yielded larger IONPs and cluster formation, synthesised IONPs exhibited rather random morphologies not resembling nanoflowers (see **Figure S9** and **Figure S10**). This was another reminder that batch procedures cannot be translated directly into flow and highlights the importance of synthesis conditions, such as heating rate, mixing, the activity of gaseous components (including reaction side products) in solution, total pressures, etc. for the formation of multicore nanoparticles.

The single- and two-stage syntheses indicated that IONP growth occurred via coalescence (or a partly aggregative growth mechanism). This is discussed further as the growth mechanism has several implications on the reactor design and the maximum size and minimum polydispersity that can be achieved in a scalable thermal decomposition process. For example, size focussing (due to the faster growth of smaller particles), which is well described to yield monodisperse particles for growth via surface integration of monomers or other molecular building blocks from solution,[68,74] can be expected to have a lesser effect for colloidal growth. Although aggregation of smaller particles (with small or larger particles) may be preferable, this preference might fade as particles get bigger. A reduced size focussing effect for colloidal growth would explain why polyol methods (for which a partly aggregative growth mechanism is assumed) feature higher polydispersities compared to other thermal decomposition methods in non-polar solvents. Growth via coalescence would also imply the need for different thermal decomposition process designs to tune the IONP particle size. For example, the heating rate (and the related nucleation rate) does not affect the particle size much (considering an aging step). However, higher particle/precursor concentrations, reaction times, and temperatures if favouring aggregation, would increase the particle size). A reduced aggregation likelihood of larger particles, however, would make it difficult to increase the size beyond a threshold. Note that all syntheses in the single and two-stage HTFR yielded IONPs < 10 nm and a significant size increase using the same reactor seemed challenging. Hence, a different flow process allowing self-seeded growth was designed to produce larger IONPs.

Three-stage thermal decomposition synthesis with self-seeding

Although higher temperatures and longer residence times increased the particle size, synthesising IONPs > 10 nm remained challenging. Therefore, all three temperature stages were used in combination with a self-seed growth concept (see **Figure 1**).

The first precursor solution (PS I) was fed at 0.25-0.5 ml/min through Stage 1 at 200 °C (~7 min residence time at 0.5 ml/min) and subsequently Stage 2 operated at >200 °C (~28 min residence at 0.5 ml/min). The IONP solution formed after passing Stage 1 and 2 was the seed solution (= the seed). New precursor solution (= the feed, PS II) fed at 0.25-0.5 ml/min was then mixed with the seed solution. Seed and feed mixing

happened at ~room temperature, which was possible using sufficient tubing (SS and PTFE, ca 2 ml) between the Stage 2 outlet and the Y-mixer used. To guarantee efficient seed and feed mixing, the flow was segmented (N_2 fed at 0.6 ml_s/min) after mixing but before entering Stage 3. The three-stage set-up was operated at different temperatures and the feed to seed ratios varied by the seed and feed flow rates (PS I/PS II). The pressure pump fed the precursor solutions for the seed (channel 1) and feed (channel 2). The pressure recordings of both channels confirmed a stable flow process (see **Figure S18**).

Even at low temperatures, i.e., all three stages ≤ 230 °C, the particle size increased with the feed/seed ratio (see **Figure S11**). Still, the particle size did not exceed 6 nm (RSD < 13%). This was achieved by operating Stage 2 and 3 of the three-stage set-up at higher temperatures (≥ 240 °C). A further size increase to ~8 nm (RSD < 13%) was achieved by operating at a seed/feed ratio of 0.25 ml min^{-1}/0.5 ml min^{-1} and increasing the temperature of the last stage to 260 °C. To increase the particle size even further, the Fe(acac)$_3$ concentration in the feed (PS II) was doubled from 0.033 M to 0.066 M (the seed concentration PS I remained constant). This combination of self-seeded growth at different seed/feed ratios, higher temperatures, as well as higher feed concentrations made it possible to synthesise particles up to 17 nm at RSD < 14% (see **Figure 4a**). XRD confirmed that the only crystalline phase formed via the seeded growth methods was magnetite/maghemite (see **Figure S14**).

In line with the discussed growth via coalescence, the added feed is likely to form new smaller particles first rather than lead to (additive) growth to the seeds. This also explains why adding the feed did not always result in larger particles, as the small particles formed did not always fully attach to the seeds. Growth via coalescence is also apparent from the multicore particles seen in the TEM images of SS2 X2 and SS1 X2, i.e., the IONPs formed with the highest concentration of new precursor fed relative to seed particles. The HRTEM study for SS2 X2 shows that the particles formed after adding the feed were aligned multicore clusters. A nanoflower structure can be seen viewed down the [311] zone axis (see **Figure 4b** and inset, as well as **Figure S8**), while also additional reflections are seen that do not belong to that zone axis, indicating some misalignment of the grains (red circles in the inset). At higher Stage 3 temperatures (>260 °C), these multicore structures merged to single-core particles as apparent from TEM and higher magnetisation values compared below. This merging is also observed for SS1 (Stage 3 at 240 °C) and SS2 (Stage 3 at 260 °C). This too, evidenced growth via coalescence and indicated that high temperatures are required to unify (or anneal) the aggregates formed.

The magnetisation hysteresis curves (recorded at 300 K) of the largest IONPs synthesised via the three-stage process (SS2 X2, SS3 X2) and small IONPs (S1, S3) synthesised via two stages showed that all samples were superparamagnetic (see **Figure 4c**). Normalisation using the IONP weight obtained by TGA (see **Figure S19**) yielded mass magnetisations in the range of 70-80 emu/g_{IONP}. For the ~3 nm IONPs (S1), the magnetisation reduced to 20 emu/g due to surface effects of such small particles, which have a higher fraction of surface atoms of a lower spin order.

In agreement with literature, the IONPs started to generate heat in an alternating magnetic field after exceeding 10 nm (see **Figure 4d**), with the highest SAR (180 W/g, corresponding to an ILP of 0.9 nH m^2/kg) obtained for the largest (16.9 nm) particles. This shows the potential of the (self-) seeded polyol flow method to produce IONPs for magnetic hyperthermia cancer treatment too, especially as ligand exchange is simple. The particle sizes obtained were the largest for thermal decomposition flow processes yet, and also exceeded the sizes obtained in polyol batch methods (7-10 nm).[6,39,41,42]

Despite the possibility to produce IONPs between 2 and 17 nm, i.e., a > 600 fold increase in particle volume, higher heating rates are required for magnetic hyperthermia applications. This could be achieved by further increasing the particle size via a prolonged annealing step or annealing at higher temperatures. The latter, however is expected to cause fouling issues. MP-AES analysis revealed that for the dual stage syntheses (≤ 240 °C), the Fe in the form of particles in IONP solutions equalled the precursor solutions' Fe concentration, which corresponds to a yield of 100%. A yield of ~70% for operations ≥ 260 °C indicated fouling. This is

expected as adhesion to the walls is likely to increase with temperature for the same reason that aggregation increases, i.e., thermal energy overcomes any electrostatic/solvation potential. This indicates that, despite the shown stable operation for several hours at temperatures up to 280 °C, alternatives to higher temperatures are preferable to prevent reactor fouling. In addition to longer residence times for the annealing step (at temperatures < 260 °C), higher feed concentrations or a second and/or third feed addition step are sensible to further increase the IONP size.

For the total flow rates (PS I + PS II) ≤ 1 ml/min used, the continuous self-seeded three-stage thermal decomposition synthesis produced ≤ 1.5 l/d corresponding to 3-6 g_{IONP}/d depending on the precursor solution concentrations temperature settings. To increase the production rate of the single, two and three stage HTFR several strategies can be followed, also in combination. I) Through an increase of the precursor solution flow rates compensated by longer tubes and/or larger tube diameters to keep the same (average) residence time in each temperature stage. II) Through parallelisation, i.e., running several HTFRs simultaneously. For production at constant flow rates parallelisation is possible without additional pumps, as the pressure pump can feed any number of HTFRs. III) Through combination with large scale batch or "batch like" continuous reactors such as continuous stirred tank reactors (CSTRs). Especially the annealing step could be performed, at least partly, in such systems, as the heating rate (which is what makes batch processes hard to scale) is expected to have a negligible effect once the multicore particles have formed. With one strategy or another, all syntheses yielding IONPs from 2-17 nm can be scaled-up to produce at > 10 l/d (corresponding to >30 g_{IONP}/d) using the same HFTR design fitting in a single fume hood.
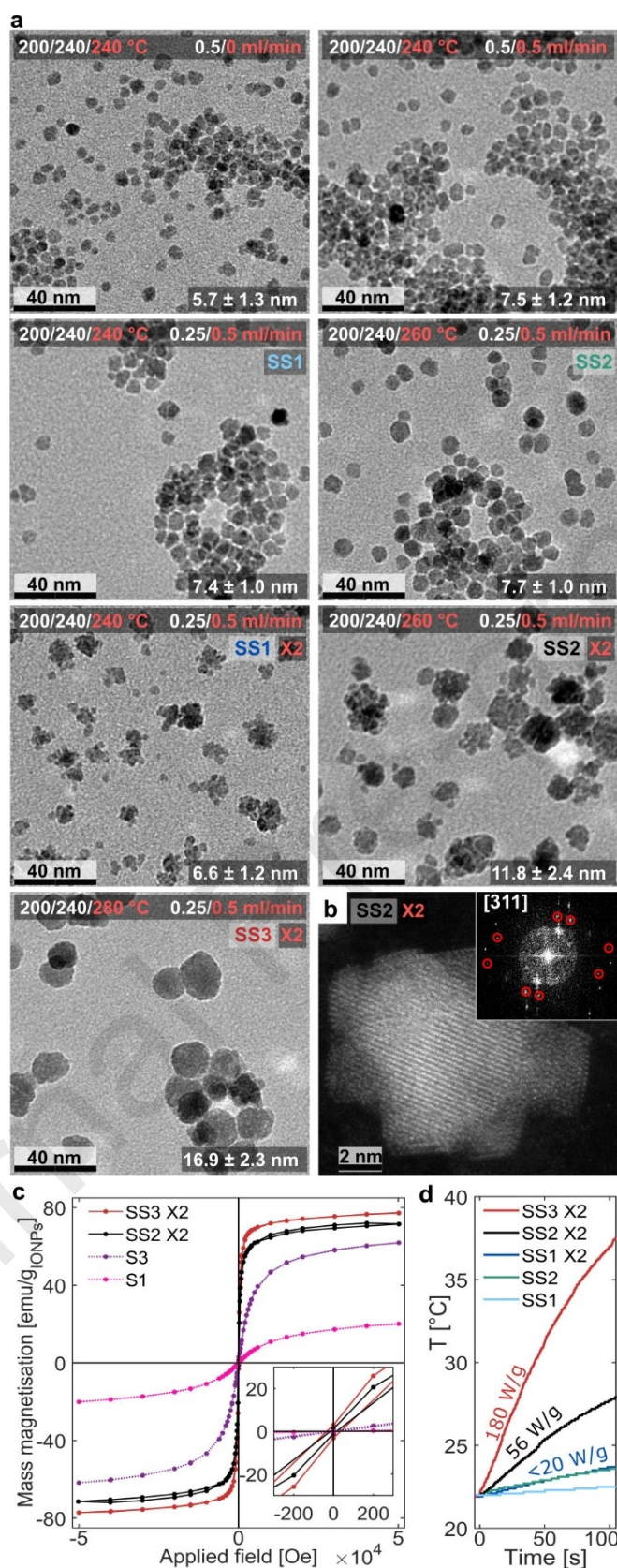
Figure 4: IONP synthesised via self-seeded three-stage process, with new precursor added before Stage 3. (**a**) TEM images of IONPs; the inset notation lists Stage 1/2/3 temperatures, flow rates PS I/PS II, and with X2 doubled PS II concentrations. (**b**) HRTEM and inserted FFT indexed to the [311] zone axis for sample SS2 X2; red circles are reflections

not belonging to that axis. (**c**) Hysteresis curves of largest and small (= S1 and S3 two-stage syntheses) IONPs. (**d**) IONP solution heating profiles with corresponding SARs.

Conclusion and perspective

A multistage, multiphase, modular high temperature flow reactor comprising 15 m of stainless steel tubing with an inner diameter of 2 mm and a fouling resistant "glass like" coating was developed to make continuous nanoparticle synthesis at high temperature possible. This reactor allows to translate the commonly used but hardly scalable high temperature nanoparticle synthesis methods into flow, i.e., facilitates large-scale production via long operation times instead of large reactor volumes. Its modularity allowed for well controlled residence times at temperatures up to 280 °C (including short exposures, i.e., < 1 min, to such high temperatures, which is not possible in batch), sharp residence profiles due to segmented flow, hence fine-tuned temperature profiles during a synthesis, as well as multiple reagent addition steps facilitating seeded growth strategies. This versatility made is possible to overcome the lack of size control in flow and synthesise nanoparticles over a broad size range. The reactor was showcased for the thermal decomposition synthesis of (magnetite/maghemite) IONPs via a simple polyol method (especially known for poor particle size control), using nothing but iron(III) acetylacetonate in triethylene glycol as precursor solution. A polyol method was chosen due to its relevance for IONP synthesis for biomedical applications, as well as its resistance to fouling which was studied in flow and batch.

The modular flow reactor concept showed potential, not only for scalable continuous production of IONPs, but also novel synthetic conditions due to rapid heating and cooling. It also provided new insights into IONP formation and growth mechanisms for polyol methods, with clear indications that growth occurred (at least partially) via coalescence. The three separated temperature stages allowed for well-defined and flexible temperature profiles as well as additional reagent addition between the stages. The three HFRT set-up configurations used, made it possible to synthesise IONPs between ~2 nm and 17 nm. i) Ultra-small ($\leq$ 3 nm) particles were synthesised using a single stage configuration heating the precursor solution to 200-220 °C for ~2 min. ii) Particles between 3 and 7 nm were obtained via the single and two-stage configuration (residence time ~22 min) and temperatures between 220 °C and 260 °C. The two-stage set-up yielded more monodisperse particles, which was attributed to a better separation between nucleation and (colloidal) growth. iii) Particles > 8 nm were synthesised via a three-stage configuration (flow rate dependent residence times < 40 min) and self-seeded growth concepts, i.e., new precursor solution (= the feed) was fed before entering the 3rd stage to the already formed particles exiting the 2nd stage. The largest particles (17 nm) were obtained using a precursor solution with a doubled $Fe(acac)_3$ feed concentration. This exceeded the largest IONPs obtained previously via any thermal decomposition synthesis in flow and exceeded the sizes obtained in polyol batch methods without subsequent autoclave step or additives. Although significantly faster than polyol batch methods (< 40 min compared to hours and days), the relative standard deviations achieved (10-15%) are similar or even lower compared to most batch protocols. Hence, monodisperse IONPs were synthesised at shorter reaction (=residence) times and the reactor concept proved worthy for scale-up via continuous production. The achieved production rates of 1-6 g_{IONP}/d can easily be increased, using the same reactor design fitting in a single fume hood, via the strategies of I) higher flow rates with longer tube lengths and/or larger diameters, II) parallelisation, or III hybrid flow-batch reactor concepts.

The flow reactor provided a unique tool for thermal decomposition synthesis of ultra-small IONPs for T_1 MRI contrast agents (as shown here) or other applications requiring a high surface-volume ratio and larger IONPs for magnetic hyperthermia. To further increase the particle size, multiple feed addition steps followed by extended (residence times > 20 min) growth steps at temperatures of ~240 °C (as well as combinations with a batch process for aging) seem most suitable.

Batch processes for thermal decomposition are hardly scalable and almost impossible to faithfully translate to flow. The particle properties depend strongly on process parameters, e.g., the heating rate, that cannot be translated directly. Hence, to facilitate reproducible and scalable nanomaterial synthesis using high

temperature methods, new procedures are required to control the particle size in flow. This was shown here, providing an engineering approach to size control.

Declaration of competing interest

The authors declare that they have no known competing financial interests or personal relationships that could have appeared to influence the work reported in this paper.

Acknowledgements

References

1   S. Rajput, C. U. Pittman and D. Mohan, *J. Colloid Interface Sci.*, 2016, **468**, 334–346.

2   X. Li, Z. Li, B. Zhu, J. Cheng, W. Li and J. Yuan, *J. Magn. Magn. Mater.*, 2021, **540**, 168472.

3   J. Li, Q. Dai, W. Huang and X. Wang, *Tribol. Int.*, 2020, **150**, 106407.

4   Q. Zhang, X. Yang and J. Guan, *ACS Appl. Nano Mater.*, 2019, **2**, 4681–4697.

5   M. Mahmoudi and S. Laurent, *Iron Oxide Nanoparticles for Biomedical Applications : Synthesis, Functionalization and Application*, Elsevier, Amsterdam, 1st edn., 2017.

6   R. Hachani, M. Lowdell, M. Birchall, A. Hervault, D. Mertz, S. Begin-Colin and N. T. K. Thanh, *Nanoscale*, 2016, **8**, 3278–3287.

7   Y. Bao, J. A. Sherwood and Z. Sun, *J. Mater. Chem. C*, 2018, **6**, 1280–1290.

8   I. Rubia-Rodríguez, A. Santana-Otero, S. Spassov, E. Tombácz, C. Johansson, P. De La Presa, F. J. Teran, M. P. Morales, S. Veintemillas-Verdaguer, N. T. K. Thanh, M. O. Besenhard, C. Wilhelm, F. Gazeau, Q. Harmer, E. Mayes, B. B. Manshian, S. J. Soenen, Y. Gu, Á. Millán, E. K. Efthimiadou, J. Gaudet, P. Goodwill, J. Mansfield, U. Steinhoff, J. Wells, F. Wiekhorst and D. Ortega, *Materials (Basel).*, 2021, **14**, 1–37.

9   D. Chang, M. Lim, J. A. C. M. Goos, R. Qiao, Y. Y. Ng, F. M. Mansfeld, M. Jackson, T. P. Davis and M. Kavallaris, *Front. Pharmacol.*, 2018, **9**, 1–20.

10   H. Etemadi and P. G. Plieger, *Adv. Ther.*, 2020, **3**, 2000061.

11   C. H. Fang, P. I. Tsai, S. W. Huang, J. S. Sun, J. Z. C. Chang, H. H. Shen, S. Y. Chen, F. H. Lin, L. T. Hsu and Y. C. Chen, *BMC Infect. Dis.*, 2017, **17**, 1–12.

12   H. Nguyen, N. Ohannesian, P. C. Bandara, A. Ansari, C. T. Deleo, D. Rodrigues, K. S. Martirosyan and W. C. Shih, *ACS Appl. Mater. Interfaces*, 2020, **12**, 10291–10298.

13   R. Tietze, J. Zaloga, H. Unterweger, S. Lyer, R. P. Friedrich, C. Janko, M. Pöttler, S. Dürr and C. Alexiou, *Biochem. Biophys. Res. Commun.*, 2015, 468, 463–470.

14   J. Huang, Y. Li, A. Orza, Q. Lu, P. Guo, L. Wang, L. Yang and H. Mao, *Adv. Funct. Mater.*, 2016, **26**, 3818–3836.

15   H. Wei, O. T. Bruns, M. G. Kaul, E. C. Hansen, M. Barch, A. Wiśniowska, O. Chen, Y. Chen, N. Li, S. Okada, J. M. Cordero, M. Heine, C. T. Farrar, D. M. Montana, G. Adam, H. Ittrich, A. Jasanoff, P. Nielsen and M. G. Bawendi, *Proc. Natl. Acad. Sci.*, 2017, **114**, 2325–2330.

16   G. Huang, H. Li, J. Chen, Z. Zhao, L. Yang, X. Chi, Z. Chen, X. Wang and J. Gao, *Nanoscale*, 2014, **6**, 10404–10412.

17   C. Blanco-Andujar, A. Walter, G. Cotin, C. Bordeianu, D. Mertz, D. Felder-Flesch and S. Begin-Colin, *Nanomedicine*, 2016, **11**, 1889–1910.

18   M. Gonzales-Weimuller, M. Zeisberger and K. M. Krishnan, *J. Magn. Magn. Mater.*, 2009, **321**, 1947–1950.

19   P. De La Presa, Y. Luengo, M. Multigner, R. Costo, M. P. Morales, G. Rivero and A. Hernando, *J. Phys. Chem. C*, 2012, **116**, 25602–25610.

20   S. Tong, C. A. Quinto, L. Zhang, P. Mohindra and G. Bao, *ACS Nano*, 2017, **11**, 6808–6816.

21   K. M. Krishnan, A. B. Pakhomov, Y. Bao, P. Blomqvist, Y. Chun, M. Gonzales, K. Griffin, X. Ji and B. K. Roberts, *J. Mater. Sci.*, 2006, **41**, 793–815.

22   M. Amini, Y. Mousazade, Z. Zand, M. Bagherzadeh and M. M. Najafpour, *Sci. Rep.*, 2021, **11**, 6642.

23   R. Hudson, Y. Feng, R. S. Varma and A. Moores, *Green Chem.*, 2014, 16, 4493–4505.

24   Z. B. Shifrina and L. M. Bronstein, *Front. Chem.*, 2018, **6**, 1–6.

25   Y. Wen, D. Jiang, A. Gavriilidis and M. O. Besenhard, *Materials (Basel).*, 2021, **14**, 6635.

26   R. K. Sharma, S. Dutta, S. Sharma, R. Zboril, R. S. Varma and M. B. Gawande, *Green Chem.*, 2016, 18, 3184–3209.

27   C. González-Fernández, J. Gómez-Pastora, E. Bringas, M. Zborowski, J. J. Chalmers and I. Ortiz, *Ind. Eng. Chem. Res.*, 2021, **60**, 16780–16790.

28   S. Laurent, D. Forge, M. Port, A. Roch, C. Robic, L. Vander Elst and R. N. Muller, *Chem. Rev.*, 2008, **108**, 2064–2110.

29   A. V. Samrot, C. S. Sahithya, J. Selvarani A, S. K. Purayil and P. Ponnaiah, *Curr. Res. Green Sustain. Chem.*, 2021, 4, 100042.

30   M. O. Besenhard, L. Panariello, C. Kiefer, A. P. LaGrow, L. Storozhuk, F. Perton, S. Begin, D. Mertz, N. T. K. Thanh and A. Gavriilidis, *Nanoscale*, 2021, **13**, 8795–8805.

31   A. E. Rawlings, L. A. Somner, M. Fitzpatrick-Milton, T. P. Roebuck, C. Gwyn, P. Liravi, V. Seville, T. J. Neal, O. O. Mykhaylyk, S. A. Baldwin and S. S. Staniland, *Nat. Commun.*, 2019, **10**, 1–9.

32   T. Hyeon, Su Seong Lee, J. Park, Y. Chung and Hyon Bin Na, *J. Am. Chem. Soc.*, 2001, **123**, 12798–12801.

33   J. Park, K. An, Y. Hwang, J.-G. Park, H.-J. Noh, J.-Y. Kim, J.-H. Park, N.-M. Hwang and T. Hyeon, *Nat. Mater.*, 2004, **3**, 891–895.

34   H. Sharifi Dehsari, A. Halda Ribeiro, B. Ersöz, W. Tremel, G. Jakob and K. Asadi, *CrystEngComm*, 2017, **19**, 6694–6702.

35   A. G. Roca, L. Gutiérrez, H. Gavilán, M. E. Fortes Brollo, S. Veintemillas-Verdaguer and M. del P. Morales, *Adv. Drug Deliv. Rev.*, 2019, 138, 68–104.

36   Z. Zhao, Z. Zhou, J. Bao, Z. Wang, J. Hu, X. Chi, K. Ni, R. Wang, X. Chen, Z. Chen and J. Gao, *Nat. Commun.*, 2013, **4**, 1–7.

37   V. Patsula, D. Horák, J. Kučka, H. Macková, V. Lobaz, P. Francová, V. Herynek, T. Heizer, P. Páral and L. Šefc, *Sci. Rep.*, 2019, **9**, 1–12.

38   E. Wetterskog, M. Agthe, A. Mayence, J. Grins, D. Wang, S. Rana, A. Ahniyaz, G. Salazar-Alvarez and L. Bergström, *Sci. Technol. Adv. Mater.*, 2014, **15**, 055010.

39   W. Cai and J. Wan, *J. Colloid Interface Sci.*, 2007, **305**, 366–370.

40   F. Fievet, S. Ammar-Merah, R. Brayner, F. Chau, M. Giraud, F. Mammeri, J. Peron, J. Y. Piquemal, L. Sicard and G. Viau, *Chem. Soc. Rev.*, 2018, **47**, 5187–5233.

41   J. Wan, R. Yuan, C. Zhang, N. Wu, F. Yan, S. Yu and K. Chen, *J. Phys. Chem. C*, 2016, **120**, 23799–23806.

42   J. Wan, W. Cai, X. Meng and E. Liu, *Chem. Commun.*, 2007, **0**, 5004–5006.

43   L. Storozhuk, M. O. Besenhard, S. Mourdikoudis, A. P. LaGrow, M. R. Lees, L. D. Tung, A. Gavriilidis and N. T. K. Thanh, *ACS Appl. Mater. Interfaces*, 2021, **13**, 45870–45880.

44   G. Hemery, A. C. Keyes, E. Garaio, I. Rodrigo, J. A. Garcia, F. Plazaola, E. Garanger and O. Sandre, *Inorg. Chem.*, 2017, **56**, 8232–8243.

45   P. Guardia, J. Pérez-Juste, A. Labarta, X. Batlle and L. M. Liz-Marzán, *Chem. Commun.*, 2010, **46**, 6108.

46   J. Van Embden, A. S. R. Chesman and J. J. Jasieniak, *Chem. Mater.*, 2015, **27**, 2246–2285.

47   A. Lassenberger, T. A. Grünewald, P. D. J. van Oostrum, H. Rennhofer, H. Amenitsch, R. Zirbs, H. C. Lichtenegger and E. Reimhult, *Chem. Mater.*, 2017, **29**, 4511–4522.

48   F. J. Douglas, D. A. MacLaren and M. Murrie, *RSC Adv.*, 2012, **2**, 8027–8035.

49   H. Gavilán, E. H. Sánchez, M. E. F. Brollo, L. Asín, K. K. Moerner, C. Frandsen, F. J. Lázaro, C. J. Serna, S. Veintemillas-Verdaguer, M. P. Morales and L. Gutiérrez, *ACS Omega*, 2017, **2**, 7172–7184.

50   M. O. Besenhard, A. P. LaGrow, S. Famiani, M. Pucciarelli, P. Lettieri, N. T. K. Thanh and A. Gavriilidis, *React. Chem. Eng.*, 2020, **5**, 1474–1483.

51 W. Glasgow, B. Fellows, B. Qi, T. Darroudi, C. Kitchens, L. Ye, T. M. Crawford and O. T. Mefford, *Particuology*, 2016, **26**, 47–53.

52 L. Uson, M. Arruebo, V. Sebastian and J. Santamaria, *Chem. Eng. J.*, 2018, **340**, 66–72.

53 M. Jiao, J. Zeng, L. Jing, C. Liu and M. Gao, *Chem. Mater.*, 2015, **27**, 1299–1305.

54 J. Mahin and L. Torrente-Murciano, *Chem. Eng. J.*, 2020, **396**, 125299.

55 T. Vangijzegem, D. Stanicki, A. Panepinto, V. Socoliuc, L. Vekas, R. N. Muller and S. Laurent, *Nanomaterials*, 2020, **10**, 757.

56 E. Bertuit, S. Neveu and A. Abou-Hassan, *Nanomaterials*, 2022, **12**, 119.

57 N. Akkurt, C. L. Altan and M. F. Sarac, *J. Supercond. Nov. Magn.*, 2022, 1–9.

58 H. Sharifi Dehsari, M. Heidari, A. Halda Ribeiro, W. Tremel, G. Jakob, D. Donadio, R. Potestio and K. Asadi, *Chem. Mater.*, 2017, **29**, 9648–9656.

59 A. Ullrich, M. M. Rahman, A. Azhar, M. Kühn and M. Albrecht, *J. Nanoparticle Res.*, 2022, **24**, 1–10.

60 B. Chen, D. Li and F. Wang, *Small*, 2020, **16**, 2002454.

61 M. L. Liu, B. Bin Chen, C. M. Li and C. Z. Huang, *Green Chem.*, 2019, 21, 449–471.

62 P. G. Jamkhande, N. W. Ghule, A. H. Bamer and M. G. Kalaskar, *J. Drug Deliv. Sci. Technol.*, 2019, 53, 101174.

63 M. J. Ndolomingo, N. Bingwa and R. Meijboom, *J. Mater. Sci.*, 2020, 55, 6195–6241.

64 Z. Li, Y. Zhang and N. Feng, *Expert Opin. Drug Deliv.*, 2019, **16**, 219–237.

65 A. V. Nikam, B. L. V. Prasad and A. A. Kulkarni, *CrystEngComm*, 2018, **20**, 5091–5107.

66 R. R. Wildeboer, P. Southern and Q. A. Pankhurst, *J. Phys. D. Appl. Phys.*, 2014, **47**, 495003.

67 J. Von Hoene, R. G. Charles and W. M. Hickam, *J. Phys. Chem.*, 1958, **62**, 1098–1101.

68 N. T. K. Thanh, N. Maclean and S. Mahiddine, *Chem. Rev.*, 2014, 114, 7610–7630.

69 J. Polte, R. Erler, A. F. Thünemann, S. Sokolov, T. T. Ahner, K. Rademann, F. Emmerling and R. Kraehnert, *ACS Nano*, 2010, **4**, 1076–1082.

70 J. Polte, *CrystEngComm*, 2015, **17**, 6809–6830.

71 G. H. Bogush and C. F. Zukoski IV, *J. Colloid Interface Sci.*, 1991, **142**, 19–34.

72 E. A. Osborne, T. M. Atkins, D. A. Gilbert, S. M. Kauzlarich, K. Liu and A. Y. Louie, *Nanotechnology*, 2012, **23**, 215602.

73 M. Jeon, M. V. Halbert, Z. R. Stephen and M. Zhang, *Adv. Mater.*, 2021, **33**, 1906539.

74 S. Mozaffari, W. Li, M. Dixit, S. Seifert, B. Lee, L. Kovarik, G. Mpourmpakis and A. M. Karim, *Nanoscale Adv.*, 2019, **1**, 4052–4066.

Declaration of interests

☒ The authors declare that they have no known competing financial interests or personal relationships that could have appeared to influence the work reported in this paper.

☐ The authors declare the following financial interests/personal relationships which may be considered as potential competing interests:
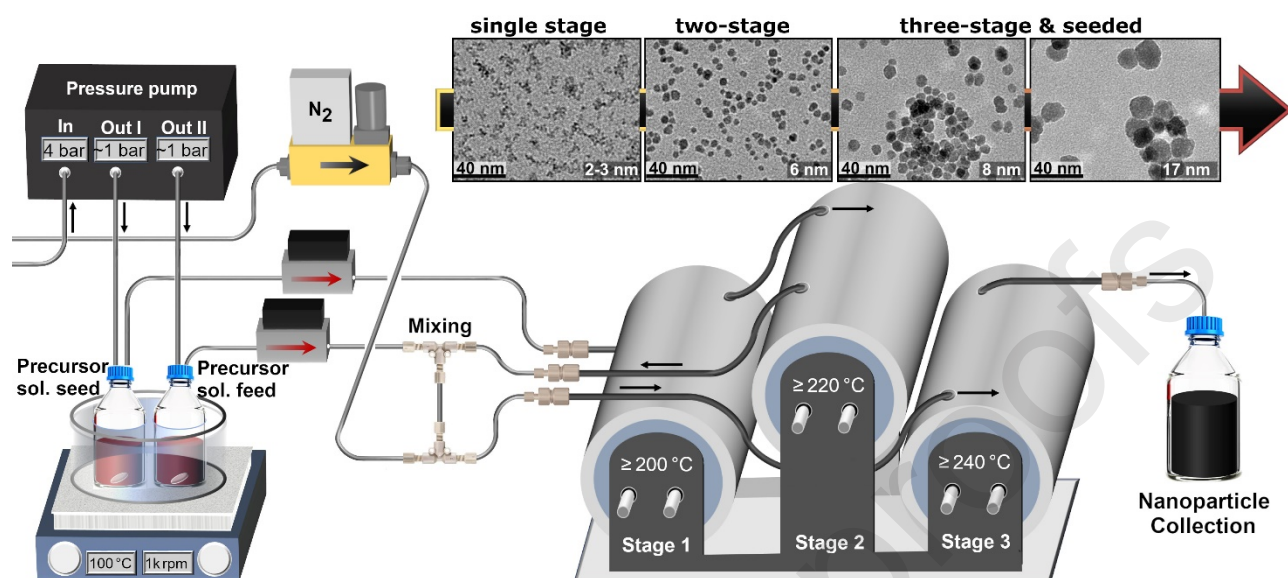
Highlights

- Versatile high-temperature flow reactor facilitating particle size control for continuous nanoparticle production
- Self-seeded growth via multistage reactor concept and particle formation mechanism study
- Iron oxide nanoparticle synthesis via continuous polyol method for biomedical applications
- Nanoparticle size tuning between 2 and 17 nm via an engineering approach for MRI T1 contrast agents and magnetic hyperthermia applications